

RESEARCH ARTICLE

Enhancing Vehicle-Machine Interface Icon Detection in Automated Testing Through a Three-Stage Machine Vision Verification Algorithm

FEI REN^{1,2,3,4}, (Student Member, IEEE), LIBING XU^{1,2,5}, JIAJIE FEI⁴,
BONIFACIO T. DOMA JR.¹ AND HONGSHENG LI⁴

¹School of Information Technology, Mapúa University, Manila 1205, Philippines

²Yanfeng Visteon Electronic Technology (Nanjing) Company Ltd., Nanjing 210000, China

³Intelligent Networking Engineering Technology Research Center, Nanjing Intelligent Transportation Information Company Ltd., Nanjing 210000, China

⁴School of Automation, Nanjing Institute of Technology, Nanjing 211167, China

⁵College of Veterinary Medicine (Institute of Comparative Medicine), Yangzhou University, Yangzhou 225000, China

Corresponding authors: Bonifacio T. Doma Jr. (btdoma@mapua.edu.ph) and Hongsheng Li (zdxhls@njit.edu.cn)

This work was supported by the University Student Science and Technology Innovation Fund Project of Nanjing Institute of Technology under Grant TB202317004.

ABSTRACT In the context of automated testing in the automotive industry, the accurate and effective detection of target icons on vehicle-machine interfaces is crucial for ensuring the efficiency and precision of automated testing processes. This paper addressed the challenge of effectively detecting vehicle-machine interface icons by proposing a three-stage verification detection algorithm based on machine vision. This paper employed an enhanced template matching technique to achieve precise positioning and initial verification of car and machine icons. Subsequently, a two-stage verification process was implemented, which focuses on detecting local changes using pixel blocks. The three-stage verification was accomplished through a three-channel separation detection of characteristic pixel points based on RGB values. Additionally, this paper utilized the collaborative capabilities of LabVIEW and OpenCV to overcome integration challenges. This joint programming approach bridged the gap between LabVIEW and OpenCV. Experimental results unequivocally underscored the paramount significance of the three-stage verification detection algorithm, rooted in the realm of machine vision. The algorithm's novel three-stage approach, intricately designed to combat background interference, not only elevated the precision of icon detection but also introduced an ingenious mechanism for classifying detection results. In this regard, it successfully overcame the limitations that have historically hindered traditional machine vision algorithms, ultimately demonstrating its paramount importance in the field of computer vision.

INDEX TERMS Vehicle-machine interface, machine vision, three-stage verification, pixel block.

I. INTRODUCTION

Template matching is recognized as one of the prominent methods in the field of image recognition. The process involves extracting multiple vectors from the target image and comparing these vectors with corresponding vectors in the template image, ultimately calculating their similarity [1].

The associate editor coordinating the review of this manuscript and approving it for publication was Abdel-Hamid Soliman^{1b}.

This method has gained acclaim and recognition in both the industrial and academic sectors for its swift detection speed and relatively modest requirements for extensive training data.

However, traditional template matching encounters inherent limitations. Firstly, its detection accuracy is lower when dealing with highly similar images, especially in distinguishing subtle changes in the scale and brightness of target objects. Secondly, the effectiveness of template matching is

significantly influenced by various factors, such as changes in the background. The consistency between the template image and the image to be detected relies heavily on it, and in industrial applications, frequent variations in background color due to data transmission can result in matching failures [2]. Template matching for target recognition had been the subject of extensive research and improvement by numerous scholars. Cheng and Lu [3] proposed a machine vision-based approach using LabVIEW Vision Assistant 2018 software for the precise localization of circular discs. The method employed template matching with vision processing algorithms to outline the shape of the discs and accurately determine their positions. However, the lack of secondary development for the LabVIEW matching algorithm had resulted in defects such as damage and deformation of the workpiece's outer contour, impacting the quality of localization and reducing the success rate and efficiency in practical applications. Addressing the issue of critical components missing in the automotive painting production field, Tao et al. [4] introduced and developed a template matching algorithm-based defect detection system for missing components. This system utilized a shape-based template matching algorithm and an image pyramid search algorithm, effectively reducing the impact of lighting and noise while ensuring real-time operation on-site. Nevertheless, the reliance on a purely shape-based template matching algorithm may limit its ability to capture detailed feature information, potentially affecting the accuracy and discriminative capability of the algorithm's detection results. Peixin et al. [5] achieved defect detection through Blob analysis, affine transformation, and NCC (Normalized Cross-Correlation) algorithm accelerated via a pyramid. This approach performed well in detecting defects in aluminum-plastic blister packaging sheets but exhibited shortcomings in detecting minor defects, indicating a need for further improvement in accuracy. Sembirng et al. [6] had used template matching in conjunction with fuzzy associative memory (FAM) to achieve real-time detection of young and old faces. This method had improved detection accuracy by 10% compared to traditional template matching. However, it had not addressed the influence of lighting and other factors on accuracy. Sriyanto et al. [7] had combined morphological processing and template matching to significantly enhance the recognition rate of Malaysian license plates. Nevertheless, this approach had struggled to effectively detect moving cars, incomplete license plates, and unclearly photographed license plates. Real-Moreno, Oscar et al. [8] introduced a novel template matching algorithm named SoRA, emphasizing faster runtime and lower computational overhead. However, there was limited attention given to the validation of false matches that may arise during the template matching process.

In this paper, the enhanced template matching method was employed to achieve precise localization and initial validation of the detection target area. Once the target area is successfully localized, the regions with overall similarity changes

are divided into blocks to undergo a dual verification process based on non-zero pixels. Additionally, RGB channel triple verification detection was applied to illuminated and off icons. Experimental results demonstrated that the improved triple verification detection algorithm, utilizing machine vision, effectively detects changes in vehicle-machine interface icons.

The integration of this series of steps enables our algorithm to dynamically and accurately select the Region of Interest (ROI), referring to the automotive interface icons to be detected, in an automated process. Subsequently, thorough validation of the selected ROI was conducted. This not only enhanced the accuracy of icon detection but also strengthened the algorithm's robustness to various environmental and image conditions. Therefore, our research had not only made theoretical advancements but has also provided a practical and reliable solution for the detection of automotive interface icons in real-world applications.

II. VEHICLE-MACHINE INTERFACE DETECTION ALGORITHM BASED ON MACHINE VISION

A. DETECTION ALGORITHM BASED ON PIXEL VALUE TEMPLATE MATCHING

Template matching, as a classic pattern recognition algorithm, has found extensive applications in various industries. This algorithm employs a statistical recognition approach to achieve target detection by defining the similarity between a template and the sample to be detected [9], [10]. During the matching process, the template image is treated as an input image block, sliding from left to right and from top to bottom on the sample image for detection. At each sliding position, the matching degree is assessed by computing the similarity, often represented using correlation coefficients [11], [12], [13], [14]. In practical industrial applications, the number of target templates is often limited, and the availability of a small data sample may not justify deep learning development. In such cases, template matching is a highly suitable method for target detection. The normalized correlation matching method is frequently used to calculate the correlation coefficient.

In this paper, the detection algorithm is developed using the OpenCV library. There are six commonly used algorithms to assess the quality of matching in template matching. Let the matrix of the template image be denoted as $T(x', y')$, the corresponding matrix of the source image as $I(x', y')$, and $R(x, y)$ as the matching metric value corresponding to each position (x, y) .

1) TM_SQDIFF

This method employs the squared difference for matching, as depicted in formula (1). The best matching outcome is when the matching value is the smallest, with larger values indicating a poorer matching result.

$$R(x, y) = \sum_{x', y'} (T(x', y') - I(x + x', y + y'))^2 \quad (1)$$

2) TM_SQDIFF_NORMED

This method utilizes the normalized squared difference for matching, as illustrated in formula (2). The optimal matching outcome is achieved when the matching value is at its smallest, and a larger matching value signifies a less favorable matching result.

$$R(x, y) = \frac{\sum_{x', y'} (T(x', y') - I(x + x', y + y'))^2}{\sqrt{\sum_{x', y'} T(x', y') * \sum_{x', y'} I(x + x', y + y')^2}} \quad (2)$$

Method 1) and method 2) are matching methods based on squared differences, and they are typically suitable for scenarios in which the template image and the image to be tested share similar external conditions and exhibit minimal grayscale variations.

3) TM_CCORR

This method utilizes the correlation matching method, as depicted in formula (3). The optimal matching outcome occurs when the matching value is at its largest, while a smaller matching value indicates a less favorable matching result.

$$R(x, y) = \sum_{x', y'} (T(x', y') * I(x + x', y + y')) \quad (3)$$

4) TM_CCORR_NORMED

This method employs the normalized correlation matching method, as described in formula (4). The most favorable matching result is achieved when the matching value is at its largest, and a smaller matching value indicates a less desirable matching outcome.

$$R(x, y) = \frac{\sum_{x', y'} (T(x', y') * I(x + x', y + y'))}{\sqrt{\sum_{x', y'} T(x', y')^2 * \sum_{x', y'} I(x + x', y + y')^2}} \quad (4)$$

Method 3) and method 4) are both correlation-based matching algorithms, and they are well-suited for scenarios with significant grayscale variations.

5) TM_CCOEFF

This method employs a correlation coefficient matching approach, which utilizes the correlation between the difference of the source image from its mean value and the difference of the template from its mean value for matching. As depicted in formula (5), the optimal matching result is achieved when the matching value is at its maximum, while the least favorable matching result occurs when the matching value is at its minimum.

$$R(x, y) = \sum_{x', y'} (T(x', y') * I(x + x', y + y')) - 1/(w * h) * \sum_{x', y'} T(x', y') * \sum_{x', y'} I(x + x', y + y') \quad (5)$$

6) TM_CCOEFF_NORMALIZED

This method utilizes the normalized correlation coefficient matching approach, as described in formula (6), as shown at the bottom of the next page. A positive value signifies a favorable matching result, while a negative value indicates a less desirable matching outcome. The larger the value, the better the matching effect.

Method 5) and method 6) are matching algorithms that rely on correlation coefficients. They exhibit robust resistance to interference and offer high accuracy when dealing with scenarios featuring minimal grayscale changes and geometric distortions. A series of test experiments have been conducted, and in this paper, method 4 is utilized for initial detection.

III. FOUR-QUADRANT VERIFICATION DETECTION BASED ON IMPROVED OTSU-TEMPLATE MATCHING

Template matching not only offers efficient computational speed but also does not require a large amount of training data. However, it carries the risk of misjudgment, often incorrectly categorizing partially similar images as consistent, resulting in highly unstable detection results [15], [16], [17], [18]. In real-world industrial applications, there is a need for enhancements to template matching.

In this paper, template matching is employed to initially identify similar areas and acquire preliminary scores. The template matching score, processed using the Otsu method, is compared with the preliminary score from the template matching, and the higher value is designated as P1. The template image and pixel area are binarized into four quadrants using the Otsu method. Non-zero pixel values and RGB values in each quadrant of the two images are individually compared to obtain scores P2 and P3. By setting thresholds for P1, P2, and P3, multiple verification detections are achieved using machine vision. This approach effectively enables the detection of similar icons, as well as distinguishing between on and off states and other potentially confusing icons on the vehicle-machine interface.

A. OTSU METHOD TO EXTRACT IMAGE FEATURES

The Otsu method segments an image into two distinct types of regions based on a threshold [19], [20], [21]. Based on histogram data, it is possible to calculate the area ratios of the foreground and background regions, which are divided by the threshold and occupy the entire image area. These area ratios are denoted as θ_1 and θ_2 . Additionally, the average gray levels corresponding to the entire image, foreground, and background are represented as μ , μ_1 , and μ_2 . The relationship between the overall average gray level of the image and the average gray levels of the two regions after division is expressed in formula (7):

$$\mu = \mu_1\theta_1 + \mu_2\theta_2 \quad (7)$$

Grayscale features within the foreground or the background are often quite similar, but the disparities in grayscale between the foreground and background are typically quite noticeable. In such cases, when there is a significant grayscale

difference between the foreground and background, the corresponding average grayscales of the two regions, μ_1 and μ_2 , will also exhibit a considerable difference compared to the overall average grayscale μ .

These differences can be effectively characterized by utilizing inter-regional variance, as expressed in formula (8):

$$\sigma_B^2(t) = \theta_1(\mu_1 - \mu)^2 + \theta_2(\mu_2 - \mu)^2 \quad (8)$$

In the formula, $\sigma_B^2(t)$ represents the variance between the foreground and the background regions obtained after the image is segmented by the threshold. Consequently, the choice of the threshold value differs, leading to distinct parameter description values for the variance between the foreground and background regions.

Expanding the formula further, the overall average grayscale, the average grayscales μ_1 and μ_2 corresponding to the foreground and background parts, and their corresponding area ratios are all functions of the threshold t , so the above formula can be extended as shown in formula (9):

$$\sigma_B^2(t) = \theta_1(t)(\mu_1(t) - \mu)^2 + \theta_2(t)(\mu_2(t) - \mu)^2 \quad (9)$$

After derivation and expansion, the inter-regional variance is shown in formula (10):

$$\sigma_B^2(t) = \theta_1(t)\theta_2(t)(\mu_1(t) - \mu_2(t))^2 \quad (10)$$

When the variance between the foreground and background regions reaches its maximum value, the difference between the two regions is the most significant, indicating the best separation state. In such cases, the threshold becomes the optimal segmentation threshold, as illustrated in formula (11):

$$T = \max[\sigma_B^2(t)] \quad (11)$$

The Otsu method utilizes the maximum variance between regions, determined from the image's own information, to automatically ascertain the threshold value. This method is characterized by its convenience and efficiency, requiring no manual parameter selection or experimentation. It can be viewed as a form of adaptive threshold selection [22], [23], [24].

B. TEMPLATE MATCHING VERIFICATION AT PRIMARY STAGE BASED ON OTSU METHOD

1) DETERMINE THE ROI AREA

Following binarization using the Otsu method, interference from the background is effectively eliminated. Template matching is then implemented based on OpenCV. The template is slid across the target detection image, and the area with the highest score is identified as the next detection target

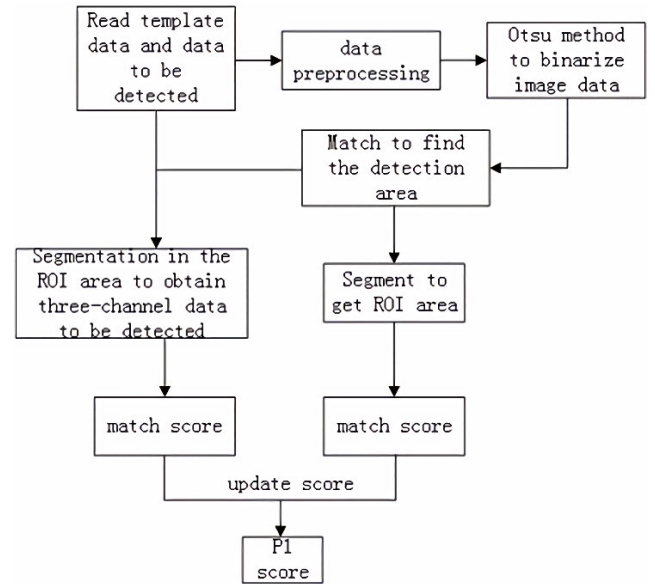


FIGURE 1. Flowchart of the matching verification algorithm in the initial stage.

area, commonly referred to as the ROI (region of interest) area. The location information of the ROI area is recorded.

2) VERIFICATION AND COMPARISON

The original image is cropped at the detection position based on the position information of the ROI area, and is then compared with the template (which reduces the time required to traverse the entire global image). The resulting score is compared with the matching score obtained after binarization using the Otsu method, and the higher score is designated as the matching score P1. Binarization by the Otsu method reduces interference information and enhances the speed of matching detection.

After obtaining the location information of the ROI area, the specific area that was not previously binarized is matched again to validate and update the score. This approach serves to shorten the detection time and bolster the detection robustness. The flowchart of the matching verification algorithm in the initial stage is illustrated in Figure 1.

C. THREE-STAGE DETECTION VERIFICATION BASED ON OTSU METHOD-TEMPLATE-FOUR-QUADRANT

The ROI area of the target image to be tested is obtained through the Otsu method-template matching verification. In practical industrial applications, there are often images with slight variations and changes in brightness when

$$R(x, y) = \frac{\sum_{x',y'} (T(x', y') * I'(x + x', y + y')) - 1/(w * h) * \sum_{x',y'} T(x', y') * \sum_{x',y'} I(x + x', y + y')}{\sqrt{\sum_{x',y'} T^2(x', y') - 1/(w * h) * (\sum_{x',y'} T(x', y'))^2} * \sqrt{\sum_{x',y'} I^2(x + x', y + y') - 1/(w * h) * (\sum_{x',y'} I(x + x', y + y'))^2}} \quad (6)$$

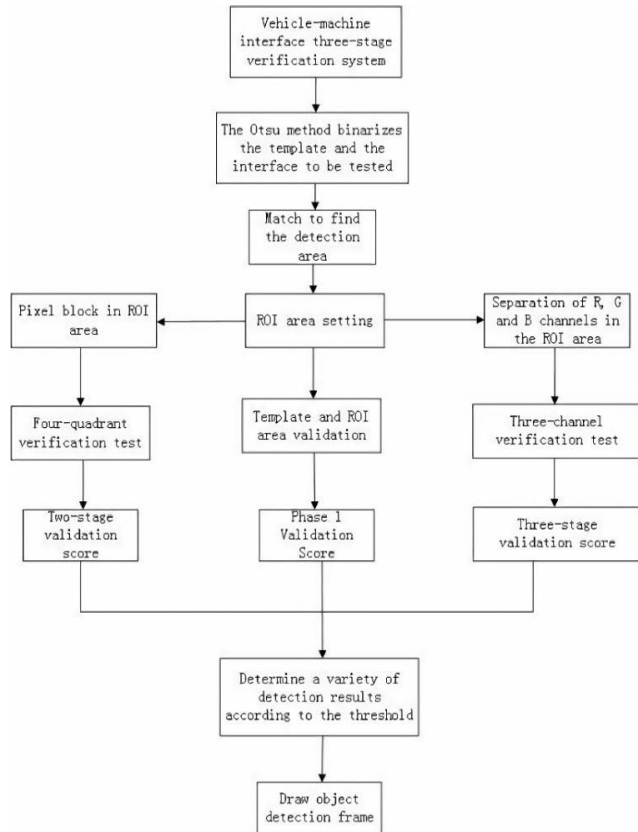


FIGURE 2. Algorithm flow of multi-level detection and verification based on Otsu method-template-four-quadrant.

icons are turned on and off. Traditional template matching algorithms may not be effectively suited for industrial production. Therefore, additional detection and verification of template images and the images to be tested are necessary [25], [26], [27].

The flow of the multi-level detection and verification algorithm based on the Otsu method-template-four quadrants, as designed in this paper, is depicted in Figure 2. Through multi-level verification and detection, it becomes possible to effectively classify similar images, and the enhanced algorithm can be reliably applied to the detection of vehicle-machine interfaces.

1) SECOND-LEVEL FOUR-QUADRANT NON-ZERO PIXEL VALUE SCORE

In this paper, the template image and the ROI area of the image to be tested are evenly divided into four sub-regions, each with a length of X_{step} and a width of Y_{step} . Specifically, X_{step} is set to half of the image width, and Y_{step} is set to half of the image height. This means that the image is divided into four quadrants, with the image center point as the origin, as depicted in Figure 3. Block detection and verification are conducted on each quadrant image, ultimately leading to the precise detection of the target area.

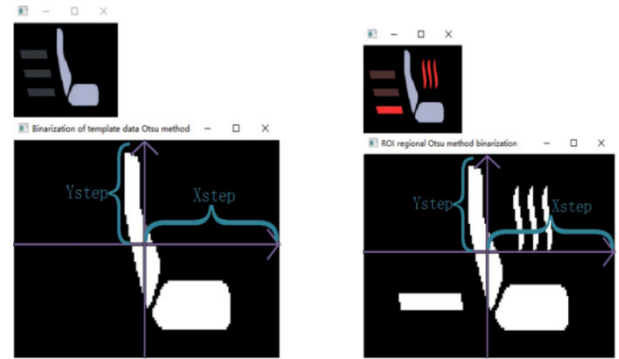


FIGURE 3. Blocked image.

In this system, for the accurate detection of target part changes, a second stage of precise detection is required, achieved through four-quadrant non-zero pixel value detection. This process is divided into the following steps:

(1) Simultaneously traverse the non-zero pixels in the first quadrant of the template image I' after Otsu's binarization and the non-zero pixels in the first quadrant of the ROI region K' of the image to be tested after Otsu's binarization. When the pixel $P(x, y)$ in the first quadrant of the I' image is not equal to 0, it is counted at this point, and the sum $x1$ of the non-zero values in the first quadrant of the I' image is calculated. Simultaneously, if the pixel $P(x, y)$ in the first quadrant of the K' image is not equal to 0, it is counted at this point, and the sum $x2$ of the non-zero values in the first quadrant of the I' image is calculated. The smaller of $x1$ and $x2$ is taken as x , and the quadrant score p' is calculated as shown in formula (12):

$$P' = \frac{|x2 - x1|}{x} \quad (12)$$

(2) Repeat step (1) in the other quadrants until all four quadrants have been traversed, obtaining four quadrant scores.

(3) The highest score among the four quadrant scores is the four-quadrant non-zero pixel value score $P2$.

2) TWO-STAGE RGB CHANNEL PIXEL VALUE VERIFICATION

In this paper, the R (Red), G (Green), and B (Blue) channels are separated between the template image and the ROI region of the image to be tested. Each channel image is detected and verified, ultimately leading to the precise detection of the target area. Figure 4 illustrates the template data and the original image of the region of interest, along with their corresponding separated R, G, and B three-channel images.

In this system, for precise detection of changes in target brightness, a third stage of accurate detection is necessary, achieved through RGB (Red, Green, Blue) pixel value detection. This process is divided into the following steps:

(1) Simultaneously traverse the R channel pixel points in the four quadrants of the original template image I and the R channel pixel values in the four quadrants of the ROI area K in the original image to be tested. Calculate the sums $y1$ and $y2$

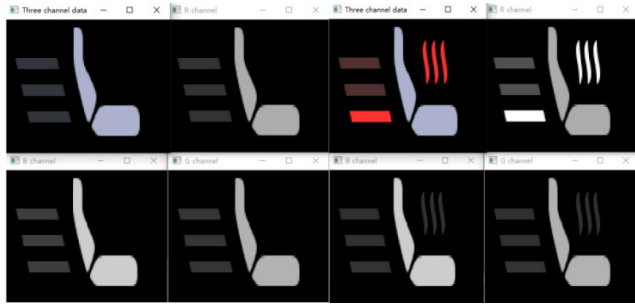


FIGURE 4. The template data and the original image of the region of interest and their corresponding separated R, G, B three-channel images.

of their values. The R channel verification score is calculated as shown in formula (13):

$$P_R = \left| \frac{y1 - y2}{Xstep * Ystep * 4} \right| \quad (13)$$

(2) Repeat step (1) in the G (Green) channel to obtain the G channel verification score.

(3) Repeat step (1) in the B (Blue) channel to get the verification score of the B channel.

(4) The highest score among the four-quadrant scores in the RGB channels is the RGB channel pixel verification value P3.

D. CLASSIFICATION OF THREE-STAGE VERIFICATION TEST RESULTS

In the processing process of this algorithm, three thresholds, T1, T2, and T3, are employed for ROI area detection in the initial stage, non-zero pixel value detection in the fourth quadrant in the second stage, and RGB channel detection and verification in the third stage. Based on the scores of P1, P2, and P3, various situations can be detected:

(1) When $P1 < T1$, it indicates that the template image is completely inconsistent with the region of interest in the data to be detected.

(2) When $P1 > T1$, the template image is similar to the region of interest in the data to be detected, and it can be further classified as follows:

a. When $P1 > T1$, $P2 < T2$, and $P3 < T3$, it means that the template image and the region of interest in the data to be detected are consistent.

b. When $P1 > T1$, $P2 < T2$, and $P3 > T3$, it suggests that the template image and the region of interest in the data to be detected differ in brightness (the icon is on and off).

c. When $P1 > T1$, $P2 > T2$, and $P3 < T3$, it implies that the template image is generally similar to the region of interest in the data to be detected, but with some differences.

d. When $P1 > T1$, $P2 > T2$, and $P3 > T3$, it indicates that the template image is generally similar to the region of interest in the data to be detected as a whole, but some parts differ, and there are variations in brightness (the icon is on and off).

Figure 5 illustrates the flow chart of the multi-situation determination system. In the experiments, the integrated

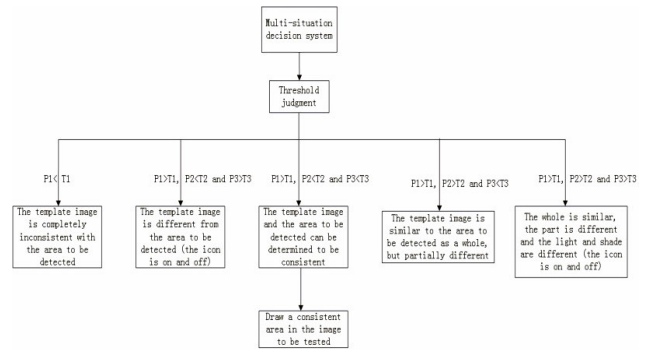


FIGURE 5. Flowchart of the multi-condition determination system.

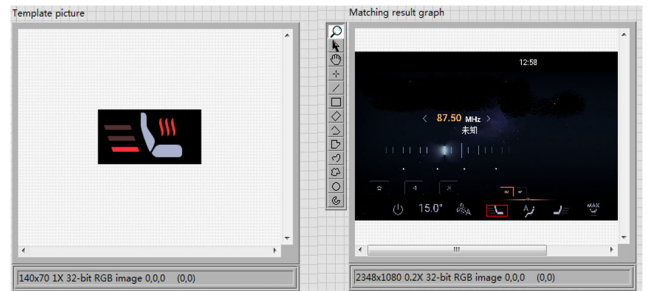


FIGURE 6. Software interface based on labview.

system’s fault tolerance and the results from a substantial amount of experimental data were set as follows: 0.95 for T1, 0.16 for T2, and 31 for T3.

IV. EXPERIMENTAL VERIFICATION

The experimental setup involves the use of a data acquisition card to capture the vehicle-machine interface. The computer platform for experimental data processing is Windows 10, with an Intel HD Graphics 5200 core graphics card, a Core i5 6200U CPU running at a frequency of 2.3GHz, and 8GB of RAM. LabVIEW is used for joint programming with the OpenCv library, creating the software interface and software operation logic. The template matching algorithm is improved using the C++ language package and is called by LabVIEW as a dynamic link library (DLL) file. Image data was collected and processed at an experimental temperature of 20 °C. The software interface is depicted in Figure 6, which highlights the matching results, and the program block diagram corresponding to the joint programming is shown in Figure 7.

In the automated testing process, the test data and results for easily confused icons in the vehicle-machine interface are presented in Table 1. This approach enables effective detection even for distorted images resulting from the capture card’s transmission process and for images that are prone to misidentification using traditional template matching.

Table 1, we observed that icons displaying overall similarity with some partial differences tend to be present on the vehicle-mounted machine interface. During real-world

TABLE 1. Main predefined styles in WORD template.














Data to be tested					
					
	Thresh-old T1	Thresh-old T2	Thresh-old T3		
	0.95	0.16	31		
template data	Score P1	Score P2	Score P3	ROI data after initial verification	judgement result
	1	0	40		P1 > T1, P2 < T2, P3 > T3: In this case, the template image differs from the region of interest in the data to be detected, indicating a difference in brightness (the icon is on and off).
	0.995	0.007	29		P1 > T1, P2 < T2, P3 < T3: In this scenario, it can be determined that the template image and the region of interest in the data to be detected are consistent.
	0.961	0.928	44		P1 > T1, P2 > T2, P3 > T3: In this situation, it indicates that the template image is generally similar to the region of interest in the data to be detected as a whole. However, there are some differences, and variations in brightness are also present, suggesting a scenario where the icon is on and off.
	0.989	0.083	26		P1 > T1, P2 < T2, P3 < T3: In this scenario, it can be determined that the template image and the region of interest in the data to be detected are consistent.
	0.954	0.990	54		P1 > T1, P2 > T2, P3 > T3: In this case, it indicates that the template image is generally similar to the region of interest in the data to be detected as a whole. However, there are some differences, and variations in brightness are also present, suggesting a scenario where the icon is on and off.
	0.991	0.062	25		P1 > T1, P2 < T2, P3 < T3: In this situation, it can be determined that the template image and the region of interest in the data to be detected are consistent.

TABLE 1. (Continued.) Main predefined styles in WORD template.

	0.956	0.352	6		$P1 > T1, P2 > T2, P3 < T3$: In this case, it indicates that the template image is generally similar to the region of interest in the data to be detected as a whole. However, there are some differences, and variations in brightness are also present, suggesting a scenario where the icon is on and off.
	0.995	0.028	22		$P1 > T1, P2 < T2, P3 < T3$: In this case, it can be determined that the template image and the region of interest in the data to be detected are consistent.
	0.961	0.351	6		$P1 > T1, P2 > T2, P3 < T3$: In this case, it suggests that the template image is generally similar to the region of interest in the data to be detected as a whole. However, there are some differences, and variations in brightness are also present, indicating a scenario where the icon is on and off.
	0.997	0.029	22		$P1 > T1, P2 < T2, P3 < T3$: In this scenario, it can be determined that the template image and the region of interest in the data to be detected are consistent.
	0.691	0.420	101		$P1 < T1$: In this case, the template image is entirely inconsistent with the region of interest in the data to be detected.
	0.714	0.429	148		$P1 < T1$: In this situation, it indicates that the template image is entirely inconsistent with the region of interest in the data to be detected.
	0.668	0.599	99		$P1 < T1$: In this case, it indicates that the template image is entirely inconsistent with the region of interest in the data to be detected.
	0.775	0.614	111		$P1 < T1$: In this scenario, it indicates that the template image is entirely inconsistent with the region of interest in the data to be detected.

operation, the transmitted images could undergo alterations, which must be distinguished from changes in icon brightness. This necessitated a robust and accurate detection algorithm. To address this challenge, the article introduced an enhanced multi-level validation detection algorithm, which is capable of effectively identifying these variations. Furthermore, this algorithm excelled in discerning between on and off icons with minimal data, particularly when dealing with images that share a general similarity but exhibit differences, especially in the context of similar shapes.

In this study, the algorithm was validated under small sample conditions by effectively detecting situations with high similarity, slight brightness variations, and different scales of

target objects on the automotive interface. The triple verification mechanism was considered as a synergistic whole, with close interdependencies among its components. Results indicated that, in comparison to potential issues observed in current research (such as those with LabVIEW-based methods, shape-based template matching algorithms, and systems utilizing NCC algorithms), such as poor detection performance for minor defects, sensitivity to lighting and noise, and false matches, this comprehensive and flexible three-stage mechanism ensured effective monitoring of icon changes on the automotive interface in various real-world scenarios. This enhanced the algorithm's robustness and reliability.

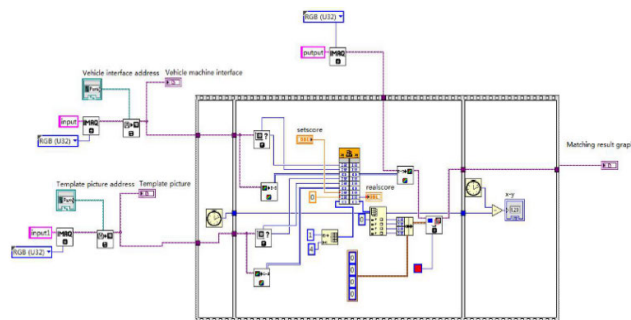


FIGURE 7. The block diagram corresponding to the Labview call detection algorithm.

V. CONCLUSION

This paper proposed a triple-verification detection method based on the joint development of LabVIEW and OpenCV, comprising improved template matching, region of interest extraction, pixel block determination, and RGB-based multi-verification detection. Traditional template matching had limitations when dealing with images exhibiting high similarity and abnormal background changes, especially concerning small-scale variations in target object size and brightness. The algorithm presented in the paper overcome these limitations through improved template matching, pixel block detection, and other steps.

Several methods in previous research suffered from poor detection performance, an inability to capture detailed feature information, and a lack of effective validation after localization. The method proposed in this paper effectively addressed these shortcomings. It successfully tackled the challenges in automotive interface detection, enhancing the accuracy of localization and scoring. Experimental results demonstrated its effectiveness in automatic visual direction detection. However, it is important to note that the threshold settings for the three-stage verification in different application scenarios significantly impact the final detection results. Further research is needed to explore adaptive threshold generation techniques for various scenarios. Additionally, the integration of OCR technology and Large Language Modeling Techniques to enhance system generalization by understanding and locating icons in images is a key focus for future research.

REFERENCES

- [1] L. Pengyu, M. Xiaoshan, and P. Xiaodong, "Ship matching detection based on simulation templates and SuperGlue," *Comput. Simul.*, vol. 40, no. 11, pp. 11–15, Nov. 2023.
- [2] M. Shuixian, Z. Chunqi, and Y. Liang, "LoRa IoT signal intelligent detection based on signal template matching," *Radio Eng.*, vol. 53, no. 12, pp. 2751–2757, Dec. 2023.
- [3] A. J. Cheng and W. Lu, "Disk recognition and positioning based on LabVIEW and its application," *J. Bengbu Univ.*, vol. 11, no. 2, pp. 36–40, Jan. 2022, doi: [10.13900/j.cnki.jbc.2022.02.008](https://doi.org/10.13900/j.cnki.jbc.2022.02.008).
- [4] C. Tao, X. Fangting, and W. Zihua, "Design and application of a template matching based system for detecting missing parts in automotive blockages," *Automot. Practical Technol.*, vol. 48, no. 24, pp. 138–141, Dec. 2023, doi: [10.16638/j.cnki.1671-7988.2023.024.027](https://doi.org/10.16638/j.cnki.1671-7988.2023.024.027).
- [5] Y. Peixin, "Research on region segmentation algorithm based on proportional features in drug plate defect detection," *Packag. Eng.*, vol. 45, no. 1, pp. 208–214, Jan. 2024, doi: [10.19554/j.cnki.1001-3563.2024.01.024](https://doi.org/10.19554/j.cnki.1001-3563.2024.01.024).
- [6] R. S. Sembiring, "Improving the accuracy of old and young face detection in the template matching method with Fuzzy Associative Memory (FAM)," *IOP Conf. Ser., Mater. Sci. Engineering*, vol. 725, no. 1, 2020, Art. no. 012117, doi: [10.1088/1757-899X/725/1/012117](https://doi.org/10.1088/1757-899X/725/1/012117).
- [7] S. Sriyanto, "Recognition of vehicle plates using template matching method," *J. Crit. Rev.*, vol. 7, no. 1, pp. 86–90, Jan. 2020, doi: [10.22159/jcr.07.01.17](https://doi.org/10.22159/jcr.07.01.17).
- [8] O. Real-Moreno, J. C. Rodríguez-Quiñonez, O. Sergiyenko, W. Flores-Fuentes, P. Mercorelli, J. A. Valdez-Rodríguez, G. Trujillo-Hernández, and J. E. Miranda-Vega, "Fast template match algorithm for spatial object detection using a stereo vision system for autonomous navigation," *Measurement*, vol. 220, Oct. 2023, Art. no. 113299, doi: [10.1016/j.measurement.2023.113299](https://doi.org/10.1016/j.measurement.2023.113299).
- [9] V. J. Maurer, M. Siggel, and J. Kosinski, "PyTME (python template matching engine): A fast, flexible, and multi-purpose template matching library for cryogenic electron microscopy data," *SoftwareX*, vol. 25, Feb. 2024, Art. no. 101636, doi: [10.1016/j.softx.2024.101636](https://doi.org/10.1016/j.softx.2024.101636).
- [10] X. Liu, X. Teng, J. Luo, Z. Li, Q. Yu, and Y. Bian, "Robust multi-sensor image matching based on normalized self-similarity region descriptor," *Chin. J. Aeronaut.*, vol. 37, no. 1, pp. 271–286, Jan. 2024, doi: [10.1016/j.cja.2023.10.003](https://doi.org/10.1016/j.cja.2023.10.003).
- [11] Q. Wang, C. Lu, L. Gao, and G. He, "Transformer-based multiple-object tracking via anchor-based-query and template matching," *Sensors*, vol. 24, no. 1, p. 229, Dec. 2023, doi: [10.3390/s24010229](https://doi.org/10.3390/s24010229).
- [12] X. Z. Ruicong and G. Xiaofeng, "Parameter estimation of multi frequency hopping signals based on improved template matching," *Electron. Inf. Warfare Technol.*, vol. 39, no. 1, pp. 30–36, Jan. 2024.
- [13] P. Xun and Y. Lei, "Action potential detection IC based on normalized template matching algorithm," *Modern Electron. Technol.*, vol. 47, no. 2, pp. 1–6, Jan. 2024, doi: [10.16652/j.issn.1004-373x.2024.02.001](https://doi.org/10.16652/j.issn.1004-373x.2024.02.001).
- [14] K. Youxin, Y. Huan, and L. Hao, "Value extraction method for electrocardiogram monitors based on peak search and template matching," *J. Biomed. Eng. Res.*, vol. 42, no. 4, pp. 337–343, Dec. 2023, doi: [10.19529/j.cnki.1672-6278.2023.04.05](https://doi.org/10.19529/j.cnki.1672-6278.2023.04.05).
- [15] L. Yutong, Z. Shanshan, and P. Lingxi, "A fast template matching algorithm based on local variance and posterior probability classification," *Appl. Electron. Technique*, vol. 46, no. 9, pp. 97–102, Sep. 2023, doi: [10.16157/j.issn.0258-7998.233881](https://doi.org/10.16157/j.issn.0258-7998.233881).
- [16] X. Zhiyong, "Research and application of template matching algorithm in image stitching," Ph.D. dissertation, Dept. Elect. CN, Nanchang Univ., Nanchang, Jiangxi, China, 2023, doi: [10.27232/d.cnki.gnchu.2023-003083](https://doi.org/10.27232/d.cnki.gnchu.2023-003083).
- [17] Y. S. Jun, Z. Zilong, and Z. Jianmin, "A chip frame image segmentation algorithm based on template matching," *Softw. Eng.*, vol. 26, no. 5, pp. 11–14, May 2023, doi: [10.19644/j.cnki.issn2096-1472.2023.005.003](https://doi.org/10.19644/j.cnki.issn2096-1472.2023.005.003).
- [18] S. Haichao, "The research on BECT spike detection algorithm based on optimal template matching and feature fusion," M.S. thesis, Dept. Hangzhou Univ. Electronic Sci. Technol., Hangzhou, China, 2023.
- [19] C. Rujie, T. Wenyan, and L. Wenge, "Multi threshold segmentation of fruit depth images based on IMFO-Otsu," *Modern Agricult. Equip.*, vol. 44, no. 4, pp. 30–35, Aug. 2023.
- [20] M. Haiyun and Z. Jinghua, "Research on classical literature text recognition algorithm based on threshold optimization technology," *J. Central Univ. Nationalities Natural Sci. Ed.*, vol. 31, no. 3, pp. 76–80, Aug. 2022.
- [21] W. Cong, L. Heng, and X. Xiaojun, "Underwater image enhancement under non-uniform lighting based on OTSU segmentation and fusion," *Optoelectronics Laser*, vol. 33, no. 1, pp. 30–36, Jan. 2022, doi: [10.16136/j.joel.2022.01.0249](https://doi.org/10.16136/j.joel.2022.01.0249).
- [22] X. Lingling, L. Qinkai, and L. Shanling, "Defect detection of electrowetting displays based on histogram gradient weighting," *Laser Optoelectronics Prog.*, vol. 58, no. 12, pp. 94–102, Jun. 2021.
- [23] X. Lihui, F. Xiaolei, and Z. Xiao, "Design of a target plate system for eliminating halo," *Mech. Electr. Eng. Technol.*, vol. 50, no. 6, pp. 46–47, Jun. 2021.
- [24] S. Mengliang, Z. Guowei, and L. Qiuhong, "A fast mismatch screening algorithm," *Mech. Eng.*, no. 3, pp. 30–32, May 2021.
- [25] B. Li, Y. Wu, F. Guo, and J. Qi, "Real-time detection method for surface defects of stamping parts based on template Matching*," *IOP Conf. Ser., Earth Environ. Sci.*, vol. 252, Jul. 2019, Art. no. 022076, doi: [10.1088/1755-1315/252/2/022076](https://doi.org/10.1088/1755-1315/252/2/022076).

- [26] X. Zhou, Y. Wang, C. Xiao, Q. Zhu, X. Lu, H. Zhang, J. Ge, and H. Zhao, "Automated visual inspection of glass bottle bottom with saliency detection and template matching," *IEEE Trans. Instrum. Meas.*, vol. 68, no. 11, pp. 4253–4267, Nov. 2019, doi: [10.1109/TIM.2018.2886977](https://doi.org/10.1109/TIM.2018.2886977).
- [27] Z. Yanling, C. Xixi, Q. Lu, and C. Pengfei, "A new fast corner detection method based on template matching," in *Proc. 2nd Int. Conf. Adv. Electron. Mater., Comput. Mater. Eng.*, vol. 563. Changsha, China, 2019, Art. no. 052093, doi: [10.1088/1757-899X/563/5/052093](https://doi.org/10.1088/1757-899X/563/5/052093).



FEI REN (Student Member, IEEE) was born in China, in 1994. He received the bachelor's degree in mechanical design, manufacturing, and automation, in 2016, and the master's degree in mechanical engineering (machine vision and artificial intelligence), in 2021. He is currently pursuing the Ph.D. degree in computer science with Mapúa University, Philippines.

He was an Off Campus Tutor for graduate students with Nanjing's universities. He has published more than ten domestic and international articles, published and authorized nearly 30 patents, won more than ten national and provincial competition awards, and published one monograph. His research interests include machine vision, machine learning, artificial intelligence, natural language processing, and OCR technology.

Mr. Ren is a member of Baidu PaddlePaddle Doctor's Association.



LIBING XU was born in China, in 1994. She received the bachelor's degree in biotechnology, in 2017, and the master's degree in aquaculture engineering, in 2020. She is currently pursuing the Ph.D. degree in bioinformatics (veterinary sanitary science) with Yangzhou University, China. Her research interests include algorithm drill and 3D model development.



JIAJIE FEI received the bachelor's degree in measurement and control technology and instrumentation from Nanjing Institute of Technology, in 2022, where he is currently pursuing the master's degree in mechanical engineering.

His research interests include machine vision, defect detection, and artificial intelligence.



BONIFACIO T. DOMA JR. received the Ph.D. degree in chemical engineering from the University of the Philippines, Diliman. He is currently a Professor of chemical engineering and business analytics. His current research interests include engineering applications of artificial intelligence and machine learning.



HONGSHENG LI was born in August 1966. He received the Ph.D. degree in engineering from the Department of Control Science and Engineering, Southeast University.

He is currently a Professor with the School of Automation, Nanjing Institute of Technology. He has led and completed more than ten important projects and multiple industry university research engineering research projects. He has published more than 70 articles in important academic journals, such as *IEEE TRANSACTIONS ON CONTROL SYSTEMS TECHNOLOGY*, *Journal of Mechanical Engineering*, *Pattern Recognition and Artificial Intelligence*, and *Information and Control*, and authorized four invention patents. His research interests include robot control, machine vision, CNC technology, and intelligent control.

...